Design and Analysis of a Flying Height Control Slider with Thermal Nanoactuator

Jia-Yang Juang and David B. Bogy

Computer Mechanics Laboratory
Department of Mechanical Engineering
University of California at Berkeley
Berkeley, CA 94720

ABSTRACT

To achieve the areal density goal in hard disk drives of 1 Tbit/in^2 the minimum physical spacing or flying height (FH) between the read/write element and disk must be reduced to ~2 nm. At such a low FH, the static and dynamic losses of the FH can cause head-disk contact and result in data loss. FH control sliders with thermal actuation have been introduced recently in commercial products for compensating the static FH loss but the inherent power-consuming thermal actuation and the strong counter effect of air bearing push-back limit its stroke. In this report we created a 3-D finite element model of an entire slider with detailed read/write transducer structure, and we conducted thermal-structural coupled-field analysis to study the actuation performance of a flying slider. An ABS design, called "Scorpion III", is proposed to achieve virtually 100 percent actuation efficiency, which is defined as the ratio of the FH reduction to actuated-pole-tip protrusion (A-PTP), with much less power consumption. A numerical study was also carried out to investigate both the static and dynamic performances of the Scorpion III slider, such as uniformity of gap FH with near-zero roll over the entire disk, ultrahigh roll stiffness and damping, low nanoscale adhesion forces, uniform FH track-seeking motion, dynamic load/unload and FH modulation

(FHM). Scorpion III was found to exhibit an overall enhancement in performance, compared with several conventional ABS designs.

1. INTRODUCTION

With the increase of areal density in hard disk drives the physical spacing (or flying height, FH) between the read/write element and the surface of the disk has been continuously decreased. A spacing of about 2.5 nm is said to be required for a density of 1 Tbit/in^2. At such a low FH static losses of the FH due to manufacturing tolerance, ambient pressure changes and temperature variations can cause head-disk contact and result in data loss. Furthermore, slider disk contacts must be avoided during load/unload processes and operational shocks. The dynamic instability caused by FH modulations (FHMs) and nanoscale adhesion forces, such as electrostatic and intermolecular forces, should be minimized. Those challenges make a conventional air bearing surface (ABS) slider an unlikely choice for 1 Tbit/in^2. One potential solution is a FH adjustment or controlled slider that is capable of adjusting its gap FH. Due to their quick response and low power consumption piezoelectric materials have been proposed as active elements for adjusting the FH [1]-[8]. However, the requirements of the piezoelectric materials and the necessary modification of the slider design pose challenges in integration of the fabrication process and increase the manufacturing cost.

The concept of adjusting the gap FH by the thermal expansion of materials was first demonstrated by Meyer *et al.* [9], in which a resistance heating element (heater) was mounted to the slider body near the read/write element. When a current is applied through the heater a portion of the head protrudes due to the mismatch of the coefficients of thermal expansion of the various materials. Such protrusion reduces the FH. Based on this concept, Kurita *et al.* developed an active head slider with a nano-thermal actuator [10]. They used a finite element method to calculate the temperature distribution and thermal protrusion of their

slider. They found that the additional air pressure increase caused by the protrusion lifted the slider upward and the amount of FH reduction was 30 % less than the protrusion. In their study the distribution of the heat transfer coefficient on the ABS was assumed to be constant. However, the effect of heat conducted from the slider to the disk through the ABS is a strong function of both FH and air pressure distributions and, hence, these two factors have to be considered in the model. Juang *et al.* [11] studied the actuation performance of an ABS slider with consideration of the effect of FH and pressure distributions. They found that even though the protruded area was relatively small, there was still considerable air bearing coupling with the resulting actuation efficiency (defined as the ratio of FH reduction to protrusion) of only 63 %, which suggested that ABS played a key role in the actuation performance. Therefore, it is highly desirable to design an ABS that can achieve high actuation efficiency (or little air bearing coupling).

In this report we present a novel ABS design for FH control sliders with a thermal nanoactuator, which can achieve high actuation efficiency, high negative pressure, high air bearing stiffness, and damping. Numerical studies of the static and dynamic performances, including flying attitude, actuation efficiency, nanoscale adhesion forces, track-seeking motion, dynamic load/unload and FHM, are carried out and discussed. The results are also compared with conventional ABS designs.

2. DESIGN CONCEPT

The concept of adjusting the FH by actuated pole-tip protrusion (A-PTP) is illustrated in Fig. 1, where an additional heating element is embedded in the read/write head. When a current is applied through the heater a portion of the head protrudes due to the mismatch of the coefficients of thermal expansion of the various materials. Such A-PTP reduces the FH.

The proposed ABS design, called Scorpion III, is illustrated in Fig. 2 (a). It has two levels of etch. The recessed area with 1.7 μm etch depth creates a subambient pressure zone and a negative pressure distribution (suction force), "pulling" the slider towards the disk surface. The two side trailing pads generate a positive pressure distribution (lift force), "pushing" the slider away from the disk surface (Fig. 2 (b)). Those negative and positive pressure distributions balance with the suspension applied gram-load and moments and together determine the flying attitude, such as FH, pitch and roll, and other important characteristics, including air bearing stiffness and damping. The read/write element is located near the center of the trailing pad of the slider body. The targeted gap FH (without actuation) is 10 nm at a disk velocity of 15000 rpm. Scorpion III was designed to achieve high actuation efficiency and to meet the following requirements: (1) constant FH profile from the inner diameter (ID) to the outer diameter (OD) taking into account the skews, (2) high roll stiffness and damping, (3) reduced effect of nanoscale adhesion forces in the HDI, (4) less FH changes during track-seeking motions, (5) better dynamic load/unload performance, and (6) acceptable FHM. The features of Scorpion III include the two side-trailing pads, the microtrailing pad and the stripes on the two leading pads. The slider is primarily supported by the positive pressure forces generated by the two side-trailing pads as seen in Fig. 2 (b). The reduced area of the microtrailing pad effectively minimizes the air bearing coupling effect and the nanoscale adhesion forces, such as electrostatic and intermolecular forces. The multiple stripes create pressure gradients and increase the air film damping [12].

3. THERMAL-STRUCTURAL FINITE ELEMENT ANALYSIS

We created a finite element model of an entire picoslider with detailed read/write transducer structure including the heating element, coil, write poles, shields, photoresist layer,

undercoat insulation layer, and overcoat (Fig. 3). The heating element is located between the coil and bottom pole. A series of thermal-structural coupled-field finite element analysis have been carried out using ANSYS to study the actuation performance of the thermal nanoactuator. The material properties and thickness of each layer are shown in Table I. These values, in particular the thermal conductivity, are process-dependent and we used the data published in various papers [13]-[16]. The cooling effect of the air bearing plays a key role in this 3-D heat transfer problem. The heat transfer model and the numerical iteration approach developed in [11], [17] are adopted in this report. For air at T = 300 K and atmospheric pressure, the thermal conductivity k = 0.0263 W/m K, the mean free path λ_0 = 65 nm, and the Prandtl number Pr = 0.7. The mean free path of the air under pressure p is $\lambda = \lambda_0 p_0/p$, while the thermal conductivity k is a very weak function of pressure. The specific heat ratio γ is 1.4 and the thermal accommodation coefficient σ_T is 0.9. We assume that the disk surface is kept at the ambient temperature T_d = 25 ^oC.

Fig. 4 shows the distributions of the heat transfer coefficient, heat flux, temperature rise and A-PTP on the ABS at a heating power of 20 mW. The disk rotational speed, radial position of the head, and skew angle were 15000 rpm, 23.88 mm, -2.56 ^{o}, respectively. The FH was reduced from 10.54 to 3.65 nm with an A-PTP of 6.91 nm. A high actuation efficiency of 99.7 % is achieved. The A-PTP as a function of the heating power is shown in Fig. 5(a). A protrusion rate of 0.34 nm/mW is obtained by a linear fit of the data points while a quadratic expression has been found to be the best fit. The FH reduction produced by the A-PTP is shown in Fig. 5(b), which shows the actuation efficiency is independent of the FH.

4. STATIC ANALYSIS

4.1 Flying Attitude and Actuation Efficiency

Numerical simulations were performed using the CML Static Air Bearing Simulator, which solved the generalized Reynolds equations and determined the steady-state flying attitude, including FH, pitch, and roll. The disk radius/skew range was 17.87 mm/-15.62° to 29.89 mm/7.22° with a disk velocity of 15000 rpm. The simulation conditions and air bearing specifications are summarized in Table II. In Figs. 6 and 7 it is seen that a nearly uniform 10-nm FH is achieved with about 2 nm loss at high altitude (4500 m) and a roll angle less than 3 μrad over the disk. A relatively high negative force of 4.8 gf is achieved, which is essential to maintaining high stiffness and low sensitivity to ambient pressure change.

Fig. 8 shows the simulated FH as a function of heating power. Due to the small area of the central trailing pad and the support of the two side trailing pads, the actuation is not coupled with the air bearing pressure and a high actuation efficiency of 99.7 % is achieved. It is seen that the reduction of the gap FH is nearly proportional to the power, and the FH of the rest of the slider is nearly unchanged. Little increase in air bearing pressure near the center trailing pad is observed when the slider has a 7.5-nm A-PTP (Fig. 9).

4.2 Stiffness and Damping of the Air Bearing

The air bearing stiffness and damping of a particular slider design are primarily determined by the geometry of the air bearing surface. It has been shown that high stiffness and damping are desired for a reliable and stable HDI. Modal analysis and the System Identification Method were used to calculate the frequency responses and obtain the modal parameters, such as modal stiffness, damping ratios and nodal lines, of the air bearing slider

[12]. Fig. 10 compares the frequency responses of Scorpion III and a conventional ABS, Slider A. It is seen that Slider A exhibits a typical three-peak curve, corresponding to the roll, first pitch and second pitch modes while Scorpion III shows only two peaks, which clearly indicates that the damping ratio for the roll mode is very large. Comparisons of the modal frequencies, stiffness and damping ratios with published data in [18]-[20] are shown in Fig. 11 and Table III. Among the four ABS designs, Scorpion III shows a remarkable increase of 294 % in damping ratio over the second most highly-damped ABS II for the roll mode (Fig. 11). As shown in Table III, Scorpion III exhibits twelve-fold increase in the roll stiffness over Slider A and 37 % and 45 % increases of the first and second pitch stiffnesses, respectively. It will be demonstrated in the Dynamic Analysis section that the dynamical performance of Scorpion III is greatly enhanced, which is primarily attributed to the significant increase of the roll stiffness and damping.

4.3 Nanoscale Adhesion Forces

Nanoscale adhesion forces, such as electrostatic and intermolecular forces, can cause dynamical instability in the HDI of ultralow flying sliders [21]. Even though those forces cannot be completely attenuated, their effect can be reduced by simply decreasing the effective slider area within proximity of the disk. For a FH control slider, this reduction in area is achieved by flying at a higher FH and actuating the read/write elements close to the disk. Numerical simulations were performed to investigate the effect of such forces on the flying attitude of Scorpion III. Fig. 12 shows the minimum FH as a function of electrostatic potential between the slider and the disk for three different ABS designs, where the 4.5-nm minimum FH of Scorpion III at zero voltage is obtained with a 5.5-nm actuation stroke. It is seen that the breakdown voltage of Scorpion III (with 124 μrad pitch) is 62 % and 83 %

higher than the high-pitch slider (245 μrad) and low-pitch slider (190 μrad), respectively. Similarly, in comparing the intermolecular force, Scorpion III exhibited 30–40 % decrease within the 2–4 nm FH region as shown in Fig. 13.

5. DYNAMIC ANALYSIS

The air bearing film and slider body form a complex coupled nonlinear dynamical system. The CML Dynamic Air Bearing Simulator is used to solve the generalized Reynolds equations coupled with the dynamics of the slider body and a lumped parameter suspension, where the suspension is represented by flexure stiffness and damping coefficients. By using the simulator we can obtain dynamic responses of a slider subject to various dynamic inputs, including the flying characteristics during track-seeking motion and FHM over measured disk morphology. The CML Load/Unload & Shock Simulator, developed by Bhargava and Bogy [22], is used to simulate complex dynamic responses of a slider in the load/unload process and under operational shock. This simulator is based on the Dynamic Simulator and uses more sophisticated finite-element models for the suspension and disk.

5.1 Flying Characteristics during Track-seeking Motion

Track-seeking is the process for a slider to move from one track to another. During this process, the FH changes as a result of the skew angle and the relative disk velocity, as well as the inertia force due to the slider's acceleration or deceleration in the cross track direction. Track access time is one of the important hard drive performance indices. Increasing the seek acceleration can reduce the access time. However, it also leads to larger inertial effects and adversely increases FH drops. Fig. 14 shows the track-seeking profile used in this study. The maximum acceleration is 65 G, and it takes 11 ms for seeking from

the ID to the OD or vice versa. The effective skew angle is the angle between the slider's longitudinal direction and the relative disk velocity (or air flow velocity) which is the resultant vector of the disk track linear velocity and the slider's seek velocity. The FH changes of Slider A and Scorpion III during the seek motion are shown in Fig. 15. It is seen that Scorpion III exhibits a remarkably flat FH during the entire seek profile with a maximum FH difference of about 0.1 nm near the ID, as compared with the 0.75-nm FH difference of Slider A near the MD. Since Scorpion III is insensitive to the skew angle and has an ultrahigh roll stiffness, its sensitivity to the skew angle change is significantly reduced, hence, resulting in a more uniform FH profile.

5.2 Dynamic Load/Unload Performance

Dynamic load/unload (L/UL) has been widely used in recent hard disk drives for achieving better shock resistance, lower power consumption as well as lower wear and debris. Previous research showed that the ABS design significantly affects the L/UL performance [23], [24]. The main design objectives of L/UL are: no slider-disk contact during the entire L/UL and a smooth and short unloading process. Challenges exist in both the loading and unloading processes. During the loading process, sliders may impact the disk especially at high loading velocities. In the unloading process, the air bearing positive pressure quickly responds to changes in FH and pitch, while the negative pressure generated by subambient cavities is relatively resistant to change. This results in a net negative force, which in turn causes slider-disk contact. The negative pressure therefore plays a key role in the L/UL processes. While the likelihood of contact can be decreased or eliminated by reducing the negative force, this force is beneficial for maintaining high stiffness and low fly sensitivity. Another potential solution is to use a slider with burnished or rounded corners [25]. However,

this additional corner rounding can cause sensitivity of the FH to tolerances associated with the manufacturing process. Another solution is to design an ABS with high roll stiffness so that it can avoid the undesirable roll motion during unloading. It has been shown in the previous section that Scorpion III has much higher roll stiffness compared to other conventional ABS designs. The CML L/UL & Shock Simulator was used to investigate the L/UL of Scorpion III with a finite element model for the suspension. The simulator models actuator rotation over a prescribed ramp profile. The unloading process takes place at the OD (29.89 mm, 7.22^{o}) and 15000 rpm. The displacements and the minimum clearances during unloading at 50 mm/s and 150 mm/s are shown in Fig. 16 (a). The minimum clearance drops due to the unloading process are illustrated in Fig. 16 (b). It is seen that the minimum clearance drops merely 0.2 nm even at a high velocity (Fig. 17). Fig. 18 shows the air bearing forces during unload. The lift-off forces are 0.83 and 1.17 gf at 50 mm/s and 150 mm/s, respectively. The displacement, minimum clearance and air bearing forces during the loading process are shown in Fig. 19. Similarly, there is no contact observed in the process.

5.3 Flying Height Modulation

In order to quantitatively compare the FHM of the ABS designs we measured the topography of a current “super-smooth” disk surface by use of a laser Doppler vibrometer (LDV) and used it as an external excitation in the simulations. The peak-to-peak and standard deviation (σ) of the disk roughness are 1.76 and 0.31 nm, respectively. Fig. 20 shows the comparison of the FHMs of Scorpion III and Slider A. The quantitative results are summarized in Table IV, which includes peak-to-peak and standard deviation measures of the FHM. The maximum peak-to-peak FHMs of Scorpion III and Slider A are found to be 0.35 nm (at the ID) and 0.47 nm (at the OD), respectively. Scorpion III exhibits a lower ratio

of the maximum to minimum peak-to-peak value than Slider A. In cross-comparing ABS designs at different radial positions, Scorpion III is found to have 54–62 % less FHM than Slider A at the MD and the OD but has 94 % more FHM at the ID. The higher FHM of Scorpion III at the ID is due to the relatively higher skew (-15.62°) and the minute positive pressure under the central trailing pad. Such FHM can be further suppressed by the dynamic feedback controller proposed by Juang and Bogy [6], [7].

6. CONCLUSION

This report proposes a novel ABS design, Scorpion III, for FH control sliders with a thermal nanoactuator, where the gap FH can be adjusted by applying an electrical current through a heating element near the read/write element. A three-dimensional thermal-structural coupled-field finite element analysis was carried out to study the actuated-PTP and power-consumption of a flying slider over a disk using velocity slip and temperature jump boundary conditions to model the cooling effect of the air bearing. It was found that Scorpion III exhibits virtually 100 percent actuation efficiency with a protrusion rate of 0.34 nm/mW. A uniform FH and near-zero roll angle were achieved across the disk. The FH loss at a high altitude (4500 m) was found to be ~20%, which can be readily compensated by the actuator with a pressure sensor. Scorpion III showed a remarkable increase in damping ratios and roll stiffness compared to several conventional designs, which is beneficial to better track-seeking and L/UL processes. The FH drop was reduced to ~0.1 nm during the track-seeking motion. Even though the Scorpion III has a considerable high negative force (-4.8 gf), the minimum clearance dropped merely 0.2 nm even at a high unloading velocity. The peak-to-peak FHM of Scorpion III simulated with a measured disk topography was found to be 0.17–0.36 nm. The higher value at the ID was due to the relative higher skew (-15.62°) and

the minute positive pressure under the central trailing pad. Furthermore, the nanoscale adhesion forces, such as electrostatic and intermolecular forces, were found to be much less compared to conventional designs due to the fact that the FH control slider flies relatively higher with the miniature microtrailing pad in the close proximity of the disk surface.

ACKNOWLEDGEMENT

This study is supported by the Computer Mechanics Laboratory (CML) at the University of California, Berkeley and Information Storage Industry Consortium (INSIC). J. Y. Juang has also been supported by The California State Nanotechnology Fellowship.

REFERENCES

1. C. E. Yeack-Scranton, V. D. Khanna, K. F. Etzold, and A. P. Praino, " An active slider for practical contact recording," *IEEE Trans. Magn.*, vol. 26, pp. 2478-2483, 1990.
2. M. Kurita and K. Suzuki, "Flying-height adjustment technologies of magnetic head sliders," *IEEE Trans. Magn.*, vol. 40, pp. 332-336, 2004.
3. K. Suzuki, R. Maeda, J. Chu, T. Kato, and M. Kurita, "An active head slider using a piezoelectric cantilever for in situ flying-height control," *IEEE Trans. Magn.*, vol. 39, pp. 826-831, 2003.
4. N. Tagawa, K.-I. Kitamura, and A. Mori, "Design and fabrication of MEMS-based active slider using double-layered composite PZT thin film in hard disk drives," *IEEE Trans. Magn.*, vol. 39, pp. 926-931, 2003.
5. L. Su, M. Kurita, J. Xu, K. Kato, K. Adachi, and Y. Miyake, "Static and dynamic characteristics of active-head sliders," *Tribol. Intl.*, vol. 38, pp. 717-723, 2005.
6. J. Y. Juang and D. B. Bogy, "Controlled-flying proximity sliders for head-media spacing variation suppression in ultralow flying air bearings," *IEEE Trans. Magn.*, vol. 41, pp. 3052-3054, 2005.
7. J. Y. Juang and D. B. Bogy, "Nonlinear compensator design for active sliders to suppress head-disk spacing modulation in hard disk drive," *IEEE/ASME Trans. Mechatron.*, to be published.
8. J. Y. Juang, D. B. Bogy and C. S. Bhatia, "Numerical and experimental studies of an Al_2O_3-TiC slider with a piezoelectric nanoactuator," *2006 ASME/JSME Joint Conf. on Micromechatronics for Information and Precision Equipment*, June 21-23, Santa Clara, CA.

9. D. W. Meyer, P. E. Kupinski, and J. C. Liu, “Slider with temperature responsive transducer positioning,” U. S. Patent 5,991,113, Nov. 23, 1999.
10. M. Kurita, T. Shiramatsu, K. Miyake, A. Kato, M. Soga, H. Tanaka, S. Saegusa and M. Suk, “Active flying-height control slider using MEMS thermal actuator,” *Microsyst. Technol.*, vol. 12, pp. 369-375, 2006.
11. J. Y. Juang, D. Chen, and D. B. Bogy, “Alternate air bearing slider designs for areal density of 1 Tbit/in^2,” *IEEE Trans. Magn.*, vol. 42, pp. 241-246, 2006.
12. Q. H. Zeng and D. B. Bogy, “Stiffness and damping evaluation of air bearing sliders and new designs with high damping,” *ASME J. Tribo.*, vol. 121, pp. 341-347, 1999.
13. L. Pust, C. J. T. Rea and S. Gangopadhyay, “Thermomechanical head performance,” *IEEE Trans. Magn.*, vol. 38, pp. 101-106, 2002.
14. Y. Yang, S. Shojaeizadeh, J. A. Bain, J. G. Zhu and M. Asheghi, “Detailed modeling of temperature rise in giant magnetoresistive sensor during an electrostatic discharge event,” *J. Applied Physics*, vol. 95, pp. 6780-6782, 2004.
15. Y. S. Ju, “Self-heating in thin-film magnetic recording heads due to write currents,” *IEEE Trans. Magn.*, vol. 41, pp. 4443-4448, 2005.
16. S. M. Lee and D. G. Cahill, “Thermal conductivity of sputtered oxide films,”*Physical Review B*, vol. 52, pp. 253-257, 1995.
17. L. Chen, D. B. Bogy, and B. Strom, “Thermal dependence of MR signal on slider flying state,” *IEEE Trans. Magn.*, vol. 36, no. 5, pp. 2486-2489, Sep. 2000.
18. B. H. Thornton and D. B. Bogy, “A numerical study of air-bearing slider form-factors,” *ASME J. Tribol.*, vol. 126, pp. 553-558, 2004.

19. Z.-E. Boutaghou, W. Qian, M. Olim, A. Sannino, J. Zhu, and C. Serpe, “Disc head slider with subambient pressure cavity bottom surfaces of different depths,” U.S. Patent 6,934,122 B2, August 23, 2005.
20. J. Y. Juang, D. B. Bogy, and C. S. Bhatia, “Design and dynamics of flying height control slider with piezoelectric nanoactuator in hard disk drives,” *ASME J. Tribol.*, submitted for publication.
21. V. Gupta and D. B. Bogy, “Dynamics of sub-5nm air bearing sliders in the presence of electrostatic and intermolecular forces at the head disk interface,” *IEEE Trans. Magn.*, vol. 41, pp. 610-615, 2005.
22. P. Bhargava and D. B. Bogy, “Numerical simulation of load/unload in small form factor hard disk drives,” Technical Report No. 2005-011, Computer Mechanics Lab., Department of Mechanical Engineering, University of California, Berkeley.
23. Q. H. Zeng and D. B. Bogy, “Slider air bearing designs for load/unload applications,” *IEEE Trans. Magn.*, vol. 35, pp. 746-751, 1999.
24. D. B. Bogy and Q. H. Zeng, “Design and operating conditions for reliable load/unload systems,” *Tribol. Intl.*, vol. 33, pp. 357-366, 2000.
25. M. Suk and D. Gillis, “Effect of slider burnish on disk damage during dynamic load/unload,” *ASME J. Tribol.*, vol. 120, pp. 332-338, 1998.

TABLE I
Material Properties used in the FEA [13]-[16]

Layer and Material		Young's modulus (GPa)	Thermal conductivity (W/m.K)	Coefficient of thermal expansion (x 10^{-6}/ $^{\circ}$C)	Poisson's ratio
Slider substrate	Al_2O_3-TiC	380	20	7.9	0.3
Under-coat (1.2 μm)	Al_2O_3	200	1.5	7.5	0.25
Shields (2.0 μm)	Ni-Fe	207	35	12.2	0.3
Bottom pole (1.0 μm)	Ni-Fe	207	35	12.2	0.3
Coil (2 μm)	Cu	120	395	16.5	0.33
Heater (250 nm)	Ni-Fe (thin layer)	207	30	12.2	0.3
Coil insulation (5 μm)	Photo-resist	7	0.19	51.0	0.2
Top pole (1.0 μm)	Ni-Fe	207	35	12.2	0.3
Over-coat (39.7 μm)	Al_2O_3	200	1.5	7.5	0.25

TABLE II
AIR BEARING SPECIFICATIONS AND FLYING ATTITUDES FOR SCORPION III

Slider Size (mm): 1.245 ×1.000×0.300
Crown: 9.3 nm
Camber: -2 nm
Suspension Load: 2.0 gf
Disk RPM: 15000

Radial Position (mm)	17.87 (ID)	21	23.88 (MD)	27	29.89 (OD)
Skew (°)	-15.62	-8.197	-2.56	2.768	7.22
Pitch (μrad)	115.79	119.85	121.33	121.40	120.52
Roll (μrad)	0.60	0.31	-0.39	-1.22	-2.09
Gap FH (nm)	9.79	9.95	9.99	10.04	10.12
Minimum FH (nm)	7.34	7.47	7.24	6.99	6.77
Negative Force (gf)	-4.67	-4.73	-4.77	-4.81	-4.85

TABLE III
COMPARISON OF AIR BEARING STIFFNESS OF VARIOUS ABS DESIGNS. THE DATA OF SCORPION III, IV AND SLIDER A WERE EVALUATED AT THE MD

	Scorpion III	Scorpion IV [20]	Slider A	Multi-Level Cavity [19]	ABS I [18]
Form factor	pico	pico	pico	pico	pico
Gap FH (nm)	9.99	10.05	10.65	10.23	4.80
Pitch (μrad)	121	109	126	230	214
Roll (μrad)	-0.4	-0.3	-1.4	0.5	0.8
k_z (gf/nm)	0.328	0.182	0.239	0.164	0.178
k_p (μN.m/μrad)	1.036	0.517	0.715	0.49	0.537
k_r (μN.m/μrad)	0.403	0.246	0.031	N/A	0.059
Negative force (gf)	-4.8	-3.1	-4.0	-3.9	-3.1

TABLE IV
SIMULATIONS OF FHM WITH ACTUAL MEASURED DISK TOPOGRAPHY FOR SCORPION III AND SLIDER A

	Air Bearing Design		
	Scorpion III	Slider A	Scorpion III/Slider A
ID: Peak-to-Peak (nm)	0.35	0.18	194 %
ID: σ (nm)	0.05	0.03	167 %
MD: Peak-to-Peak (nm)	0.12	0.26	46 %
MD: σ (nm)	0.02	0.04	50 %
OD: Peak-to-Peak (nm)	0.18	0.47	38 %
OD: σ (nm)	0.03	0.07	43 %
Max. p-p/min. p-p	292 %	261 %	
Max. σ/min. σ	250 %	233 %	

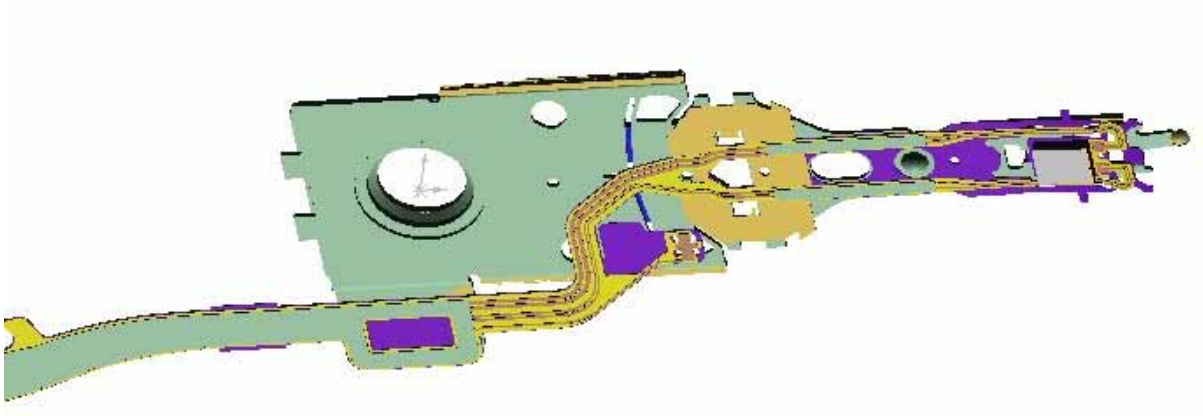

(a) Head gimbal assembly (HGA)

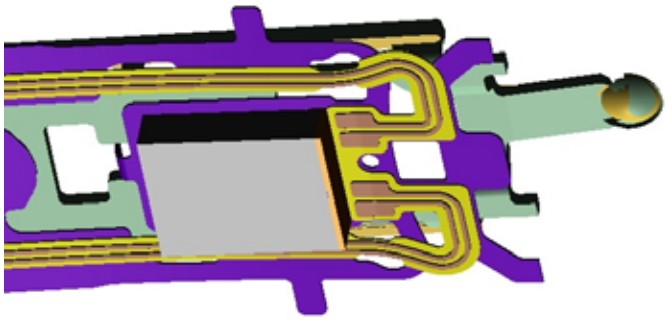

(b) Enlarged view of the slider on the suspension

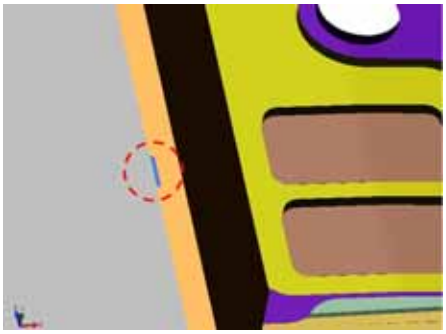

(c) the read/write elements

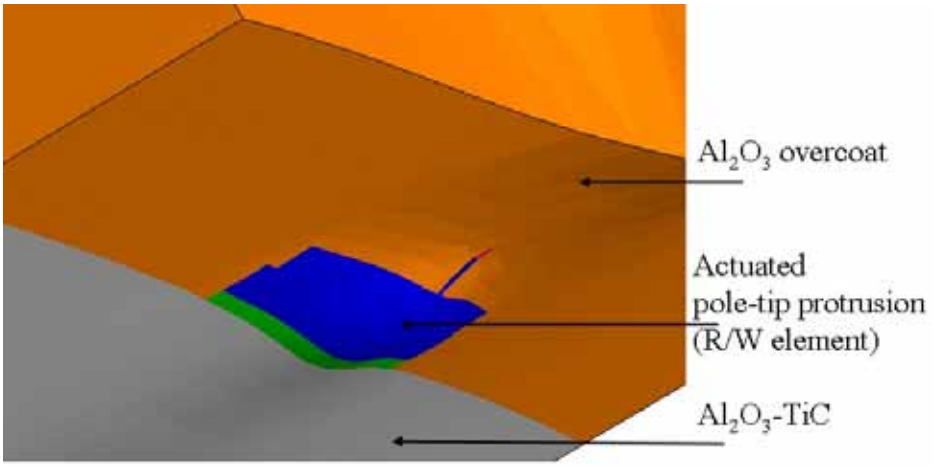

(d) perspective view of the protruded read/write elements near the trailing edge of the slider

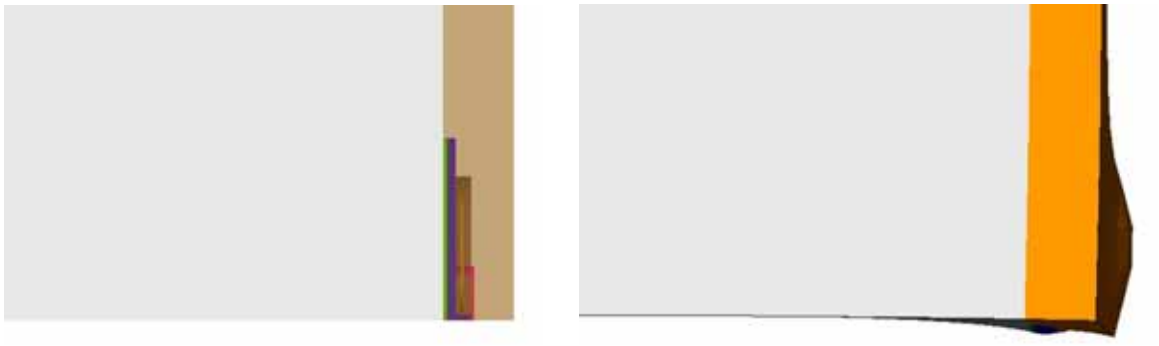

(e) without thermal actuation (f) the actuated pole-tip protrusion

Fig. 1. Schematic diagram of the actuated pole-tip protrusion of read/write elements.

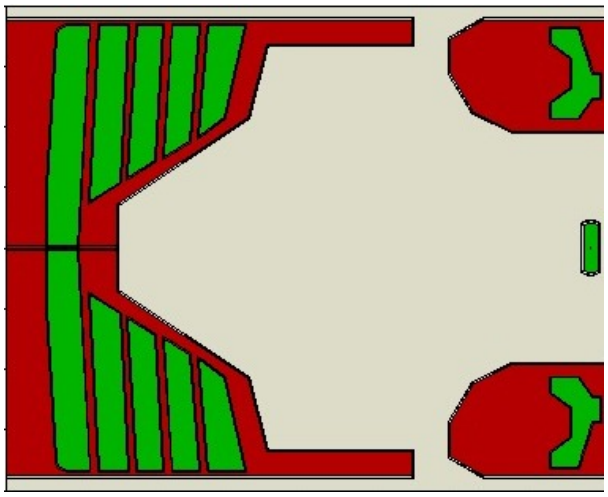

(a)

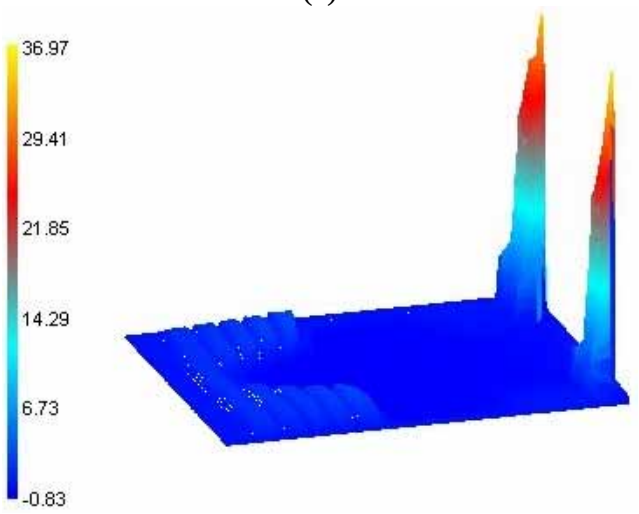

(b)

Fig. 2. (a) Air bearing surface design, Scorpion III; (b) Air bearing pressure profile at the MD (radial position 23.88 mm, skew: -2.56°). The scale displayed is normalized to ambient pressure: $(p - p_a)/p_a$.

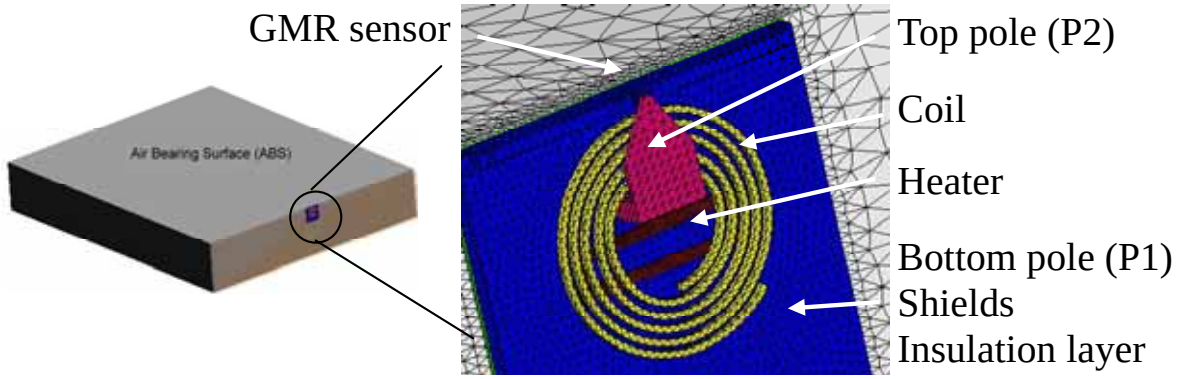

Fig. 3. The finite-element model of a slider with heating element. The overcoat and photoresist are not shown for a clear view of the read/write transducer. The thin protective carbon overcoat on the ABS is not modeled.

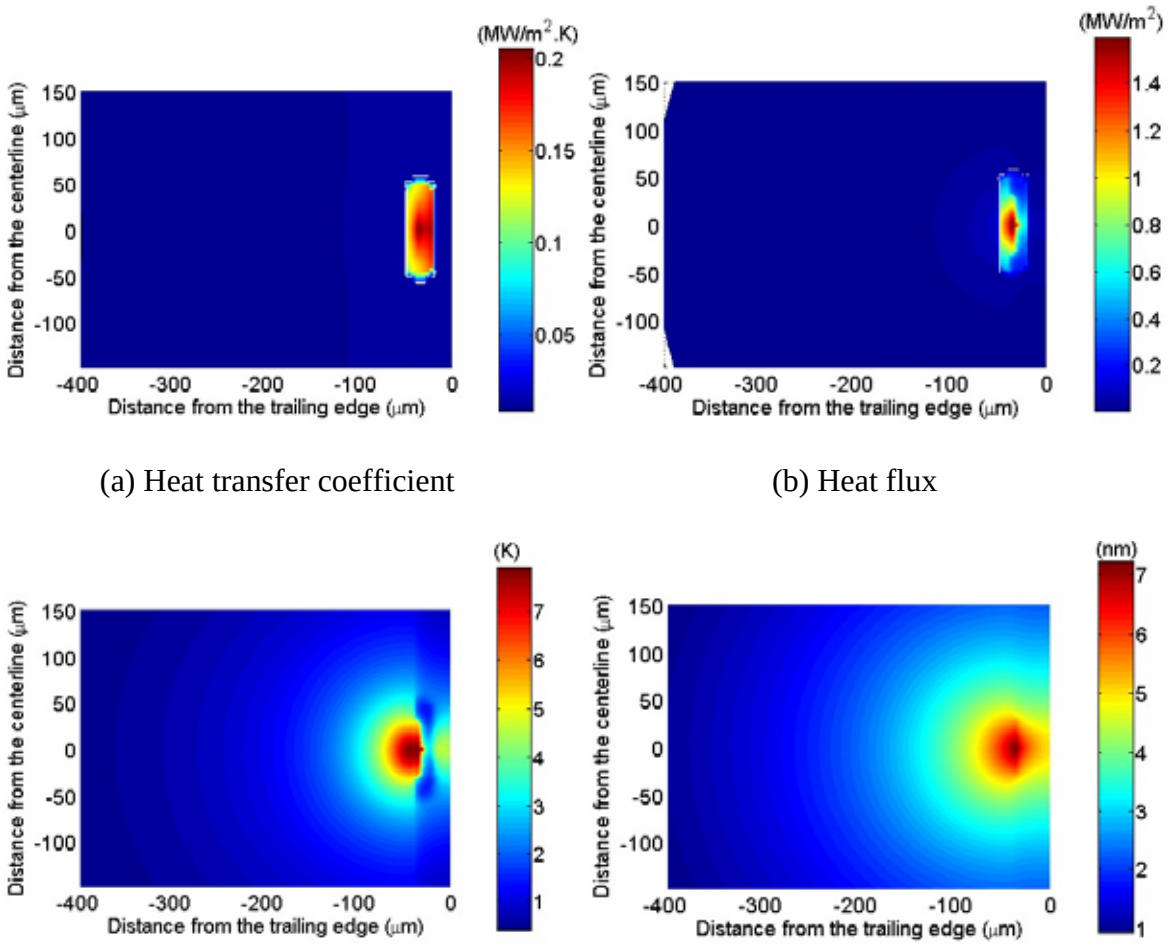

(a) Heat transfer coefficient

(b) Heat flux

(c) Temperature rise

(d) Actuated pole-tip protrusion

Fig. 4. The distributions of heat transfer coefficient (a), heat flux (b), temperature rise (c) and actuated pole-tip protrusion on the ABS near the read/write transducers.

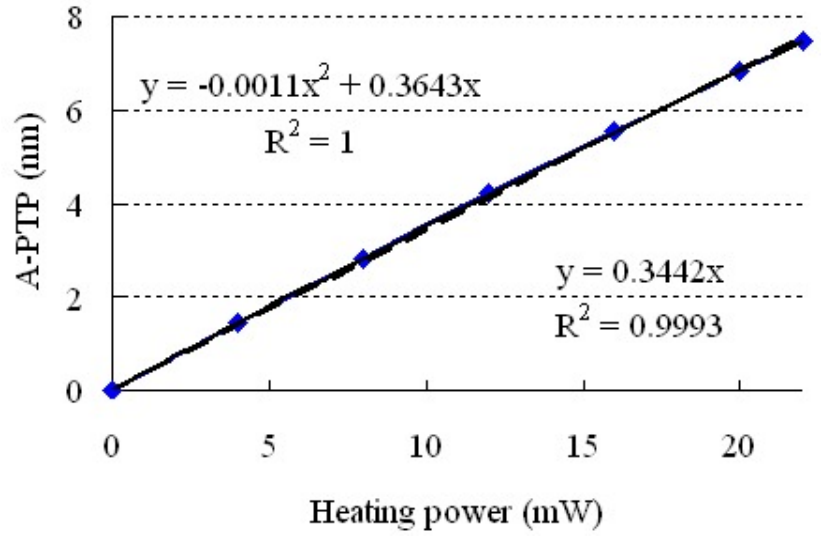

(a)

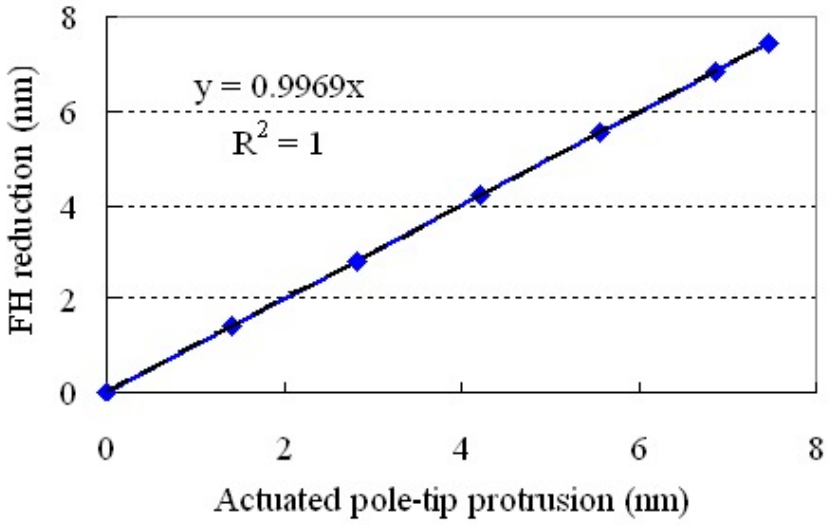

(b)

Fig. 5. (a) The A-PTP as a function of heating power; (b) the FH reduction as a function of A-PTP.

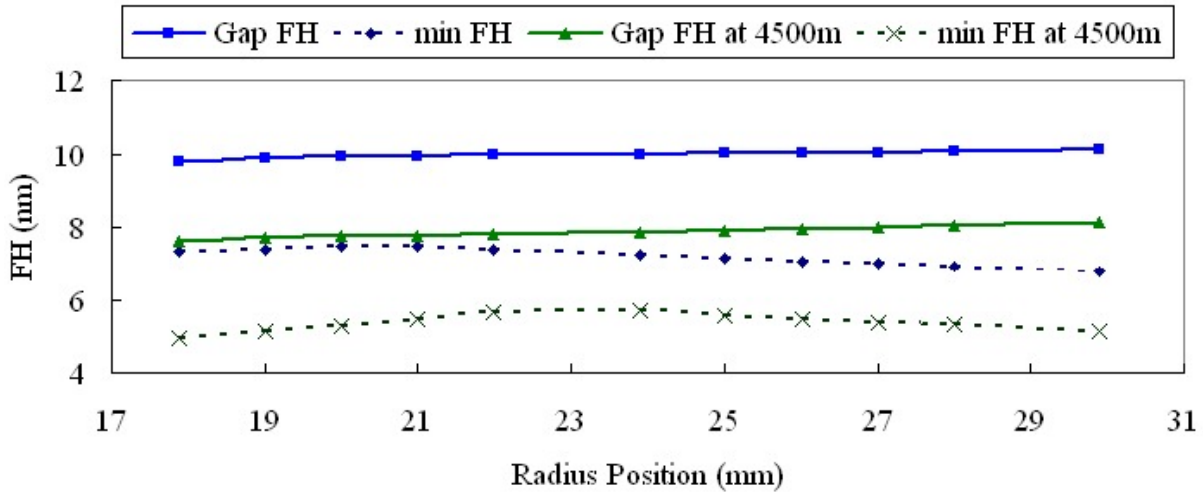

Fig. 6. Simulation of gap FH and minimum FH profiles of Scorpion III at sea level, 0 m, and high altitude, 4500 m.

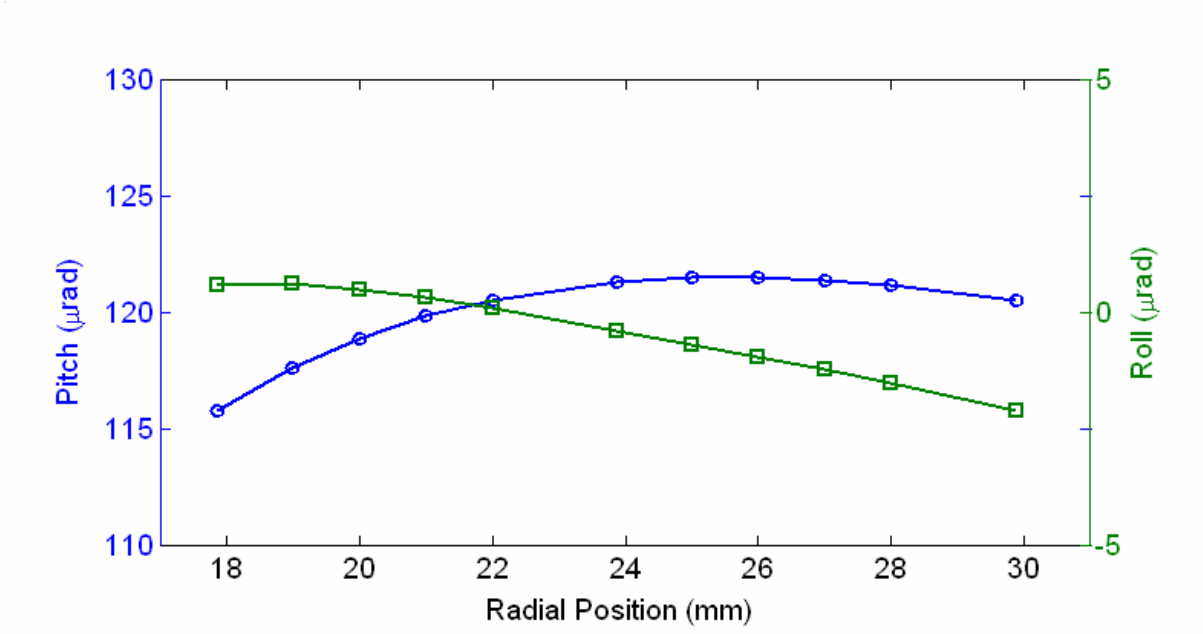

Fig. 7. Simulation of pitch and roll profiles of Scorpion III at sea level, 0 m.

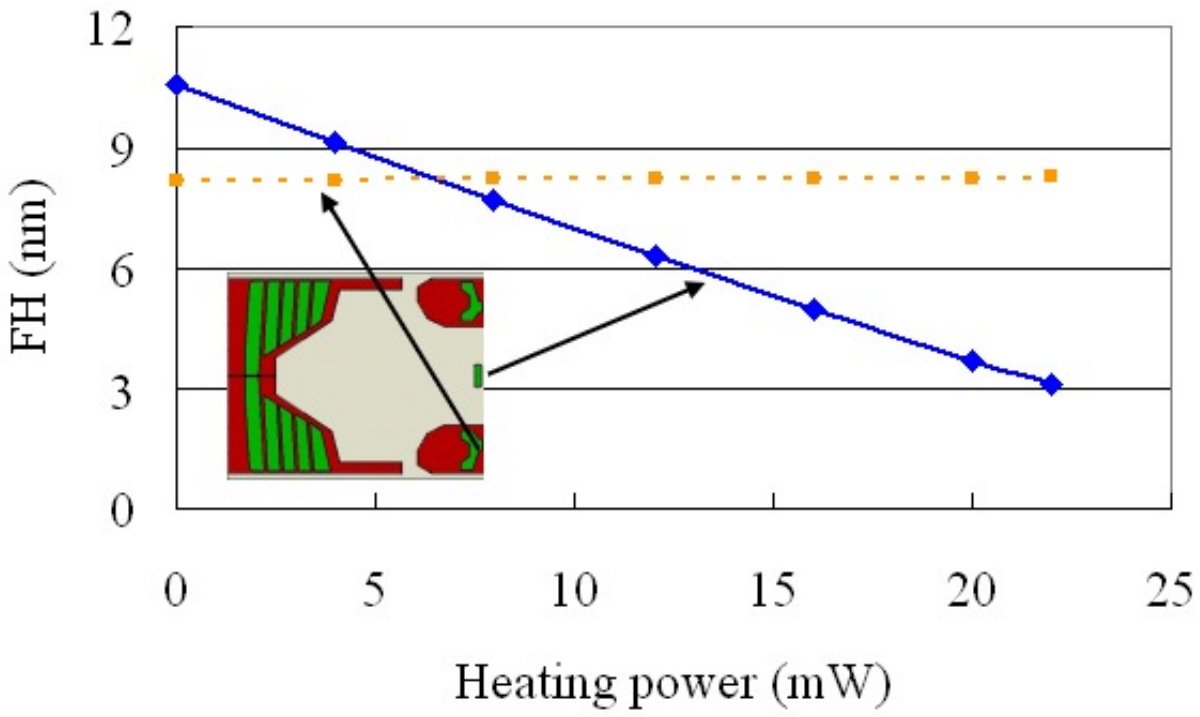

Fig. 8. Simulated FHs at the read/write transducer and one point on one of the side ABS rails. The radial position is at the MD.

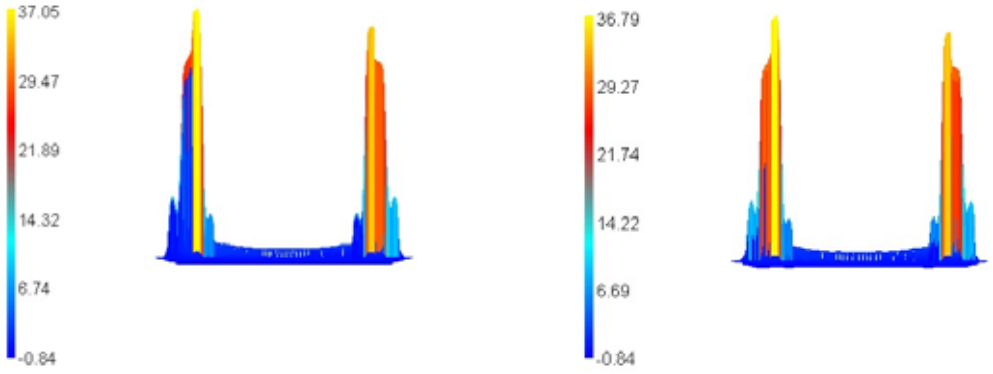

(a) (b)

Fig. 9. Air pressure distributions before (a) and after (b) a 7.5-nm actuation stroke.

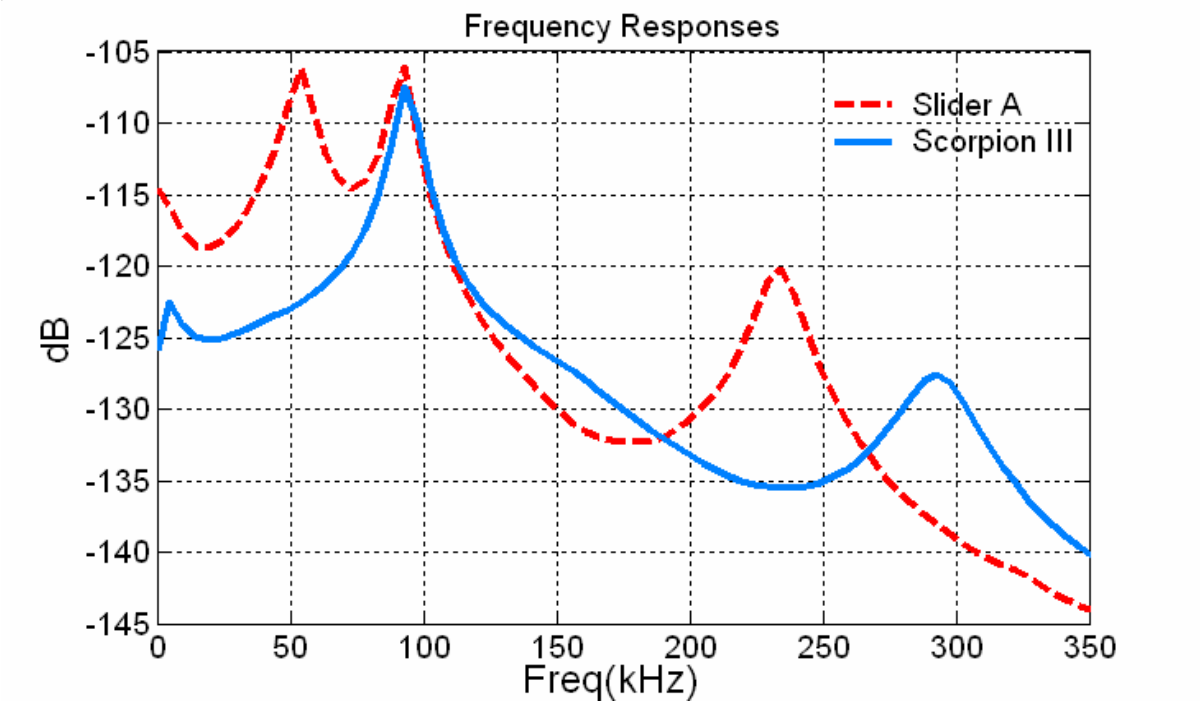

Fig. 10. Frequency responses of the air bearings of Scorpion III and Slider A.

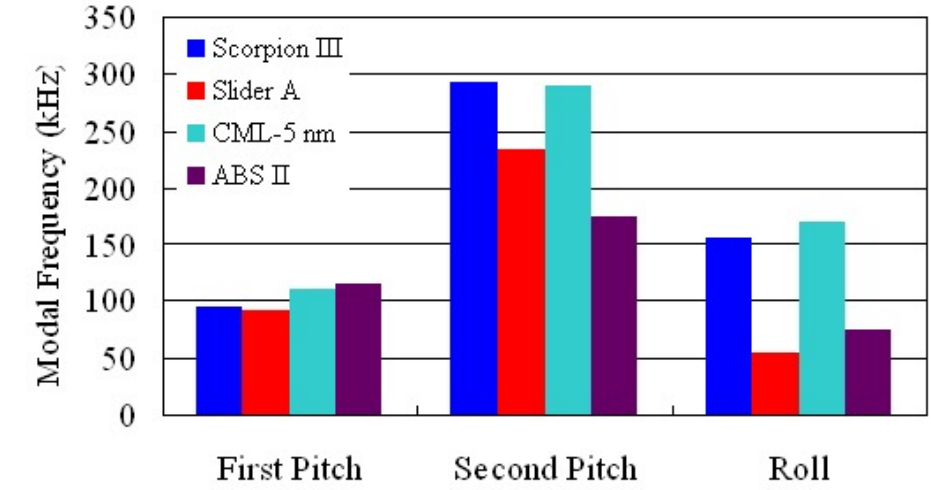

(a)

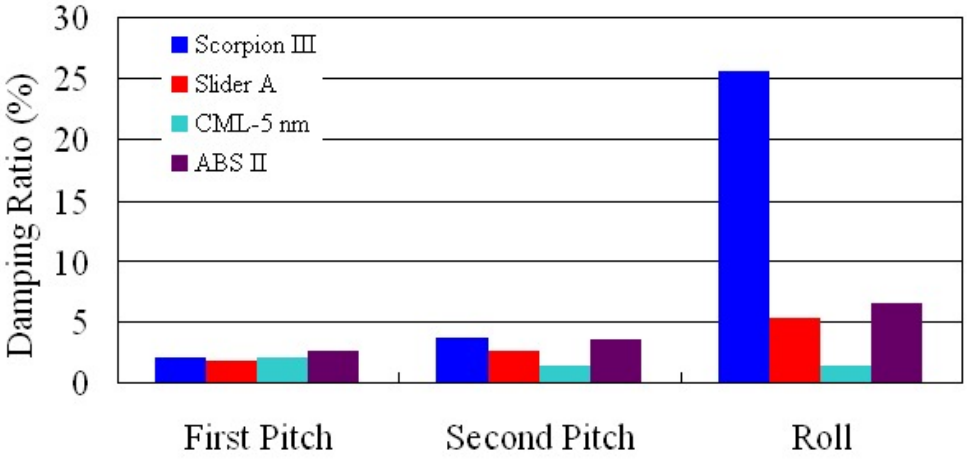

(b)

Fig. 11. Comparison of modal frequencies and damping ratios of various ABS designs. The data of Scorpion III and Slider A were evaluated at the MD. The data of CML-5nm and ABS II were obtained from [18].

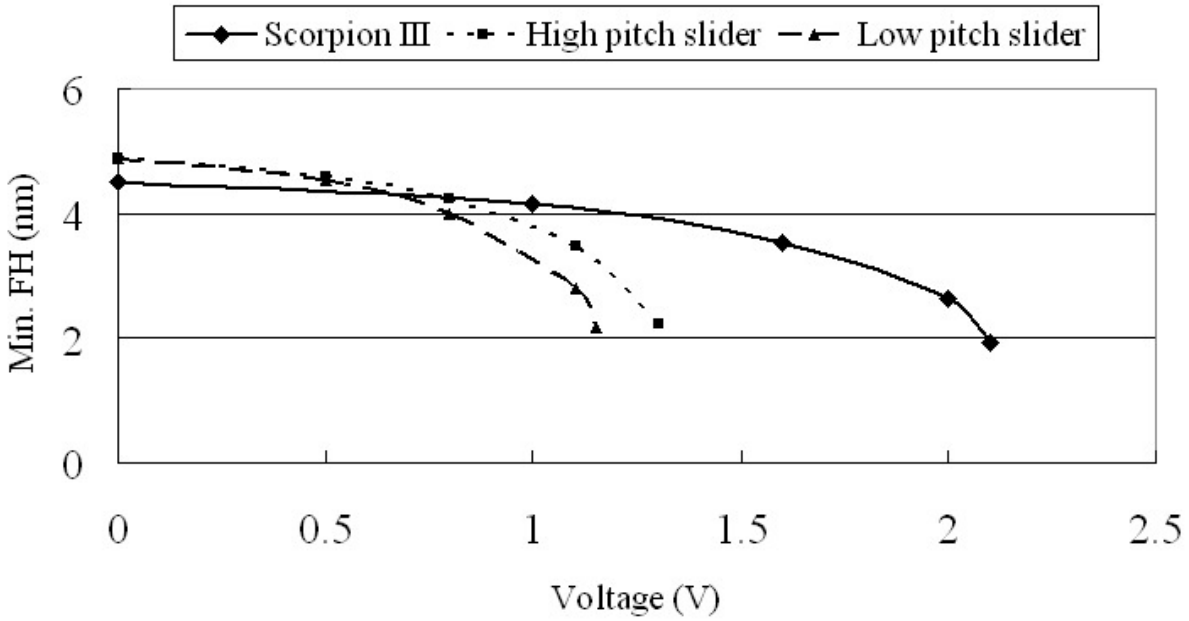

Fig. 12. The drop of minimum FH caused by the electrostatic potential across the HDI. The actuation stroke of Scorpion III is 5.5 nm. The pitch of Scorpion III is 124 μrad at zero voltage. The results of the high-pitch slider (245 μrad) and low-pitch slider (190 μrad) are from [26].

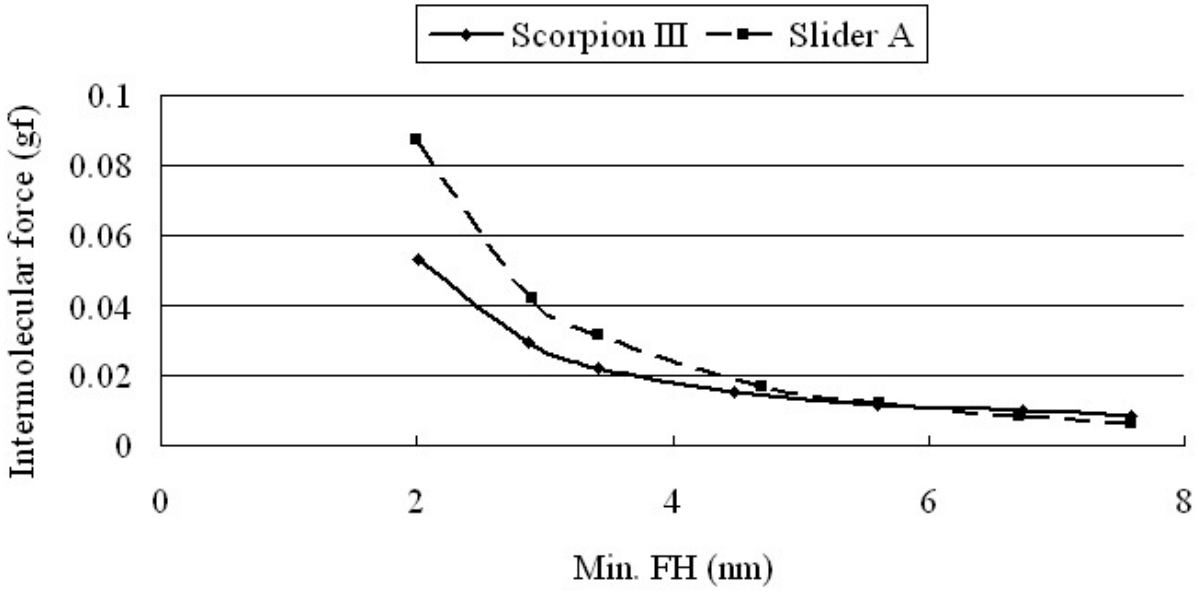

Fig. 13. Comparison of magnitudes of intermolecular adhesion forces of Scorpion III and Slider A as a function of minimum FH. The FH of Scorpion III was reduced by actuating the central trailing pad toward the disk and the obtained flying attitudes (min. FH, pitch, and roll) were then used to calculate the intermolecular forces of Slider A.

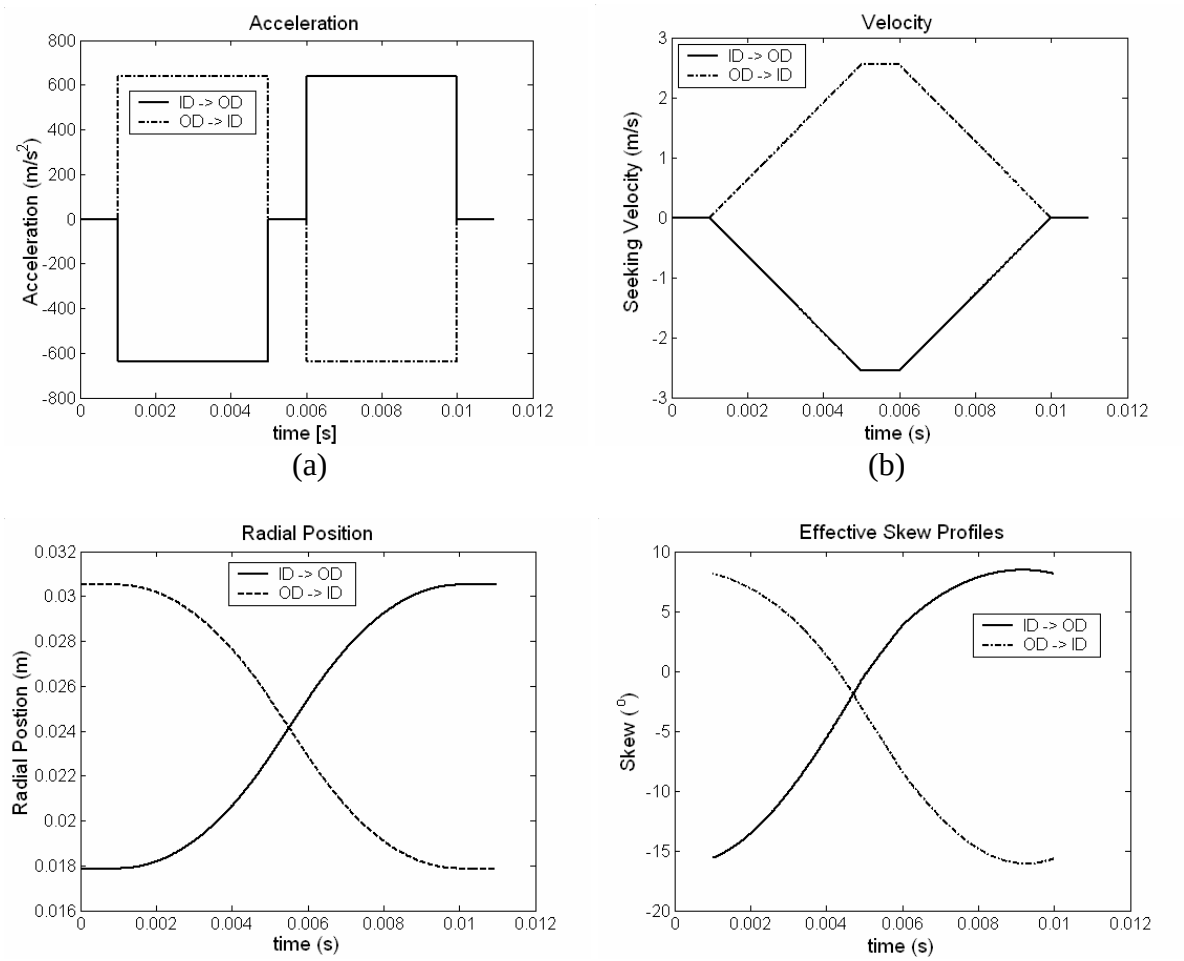

Fig. 14. Track-seeking profiles. The maximum acceleration is 65 G (637 m/s^2).

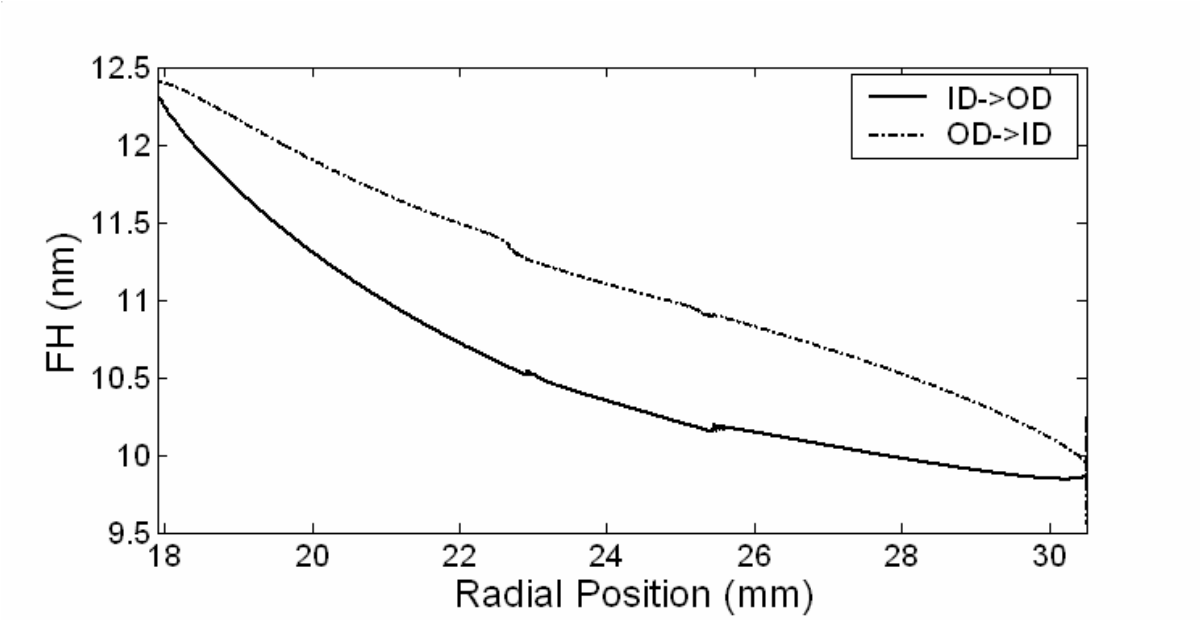

(a)

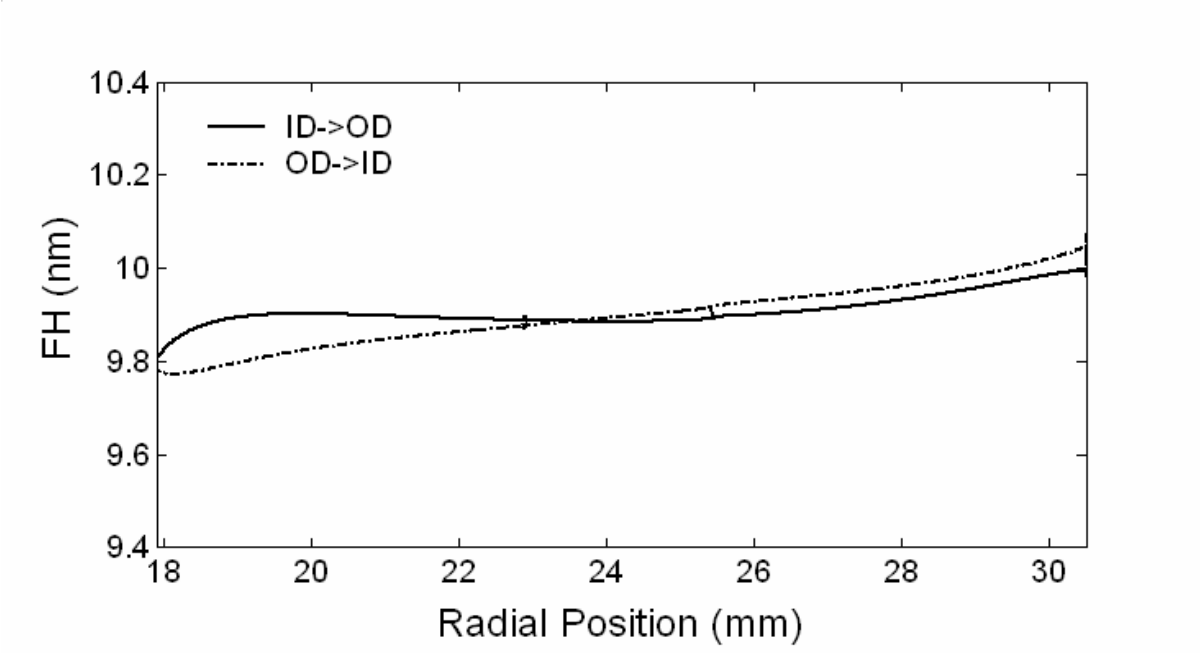

(b)

Fig. 15. Gap FH changes due to the seek motion for (a) Slider A (with a maximum difference of ~0.75 nm near the MD) and (b) Scorpion III (with a maximum difference of ~0.1 nm near the ID).

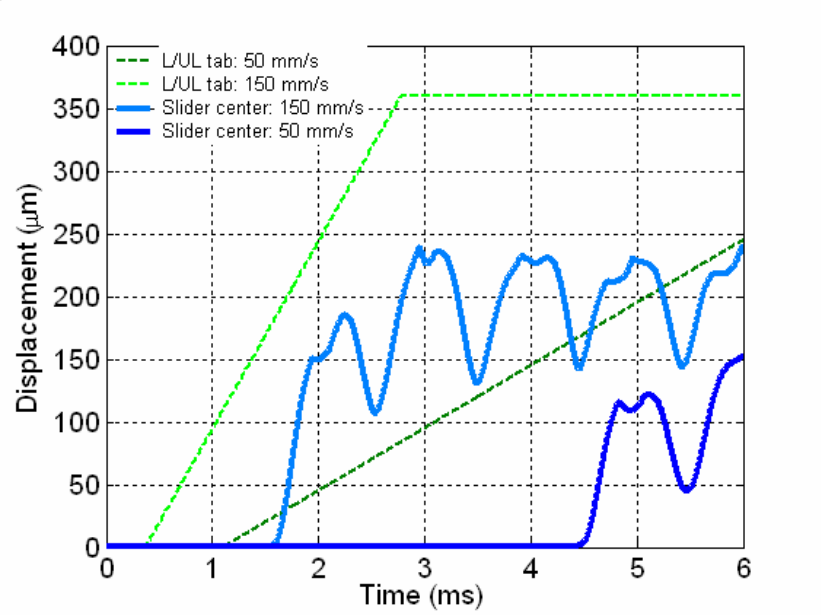

(a)

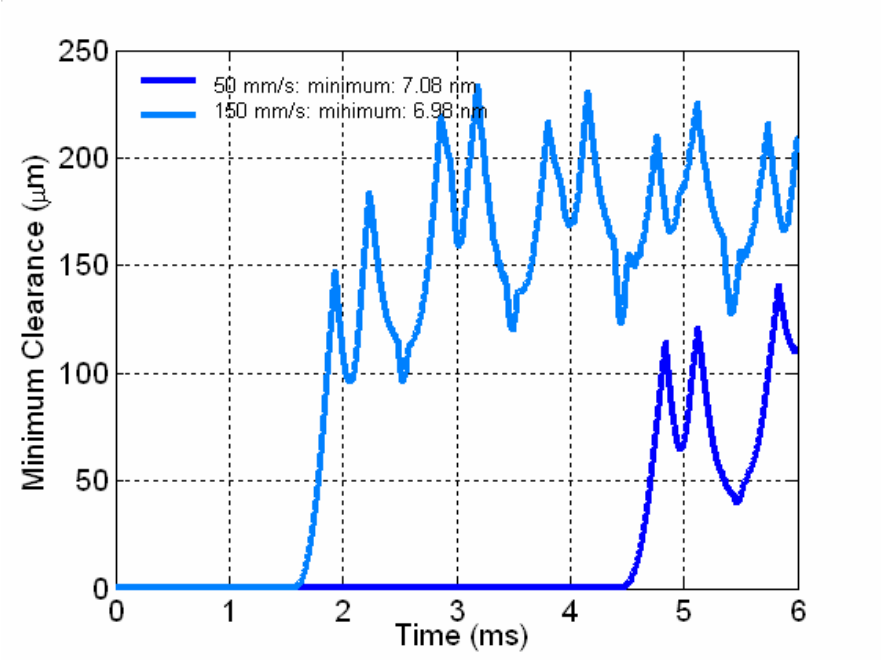

(b)

Fig. 16. Comparison of the displacement and minimum clearance histories during the unloading processes with two unloading velocities, 50 mm/s and 150 mm/s, at the OD (7.22° skew) and 15000 rpm.

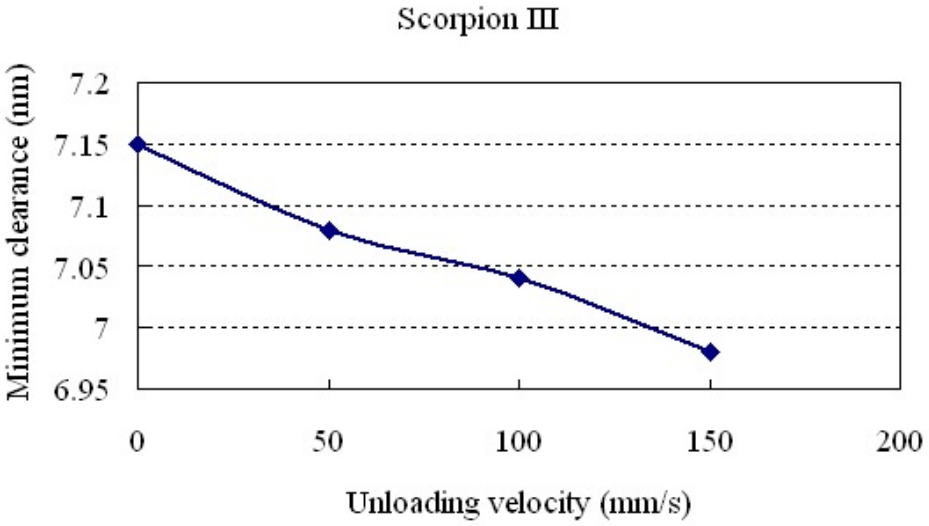

Fig. 17. The minimum clearances during the unloading process as a function of unloading velocity.

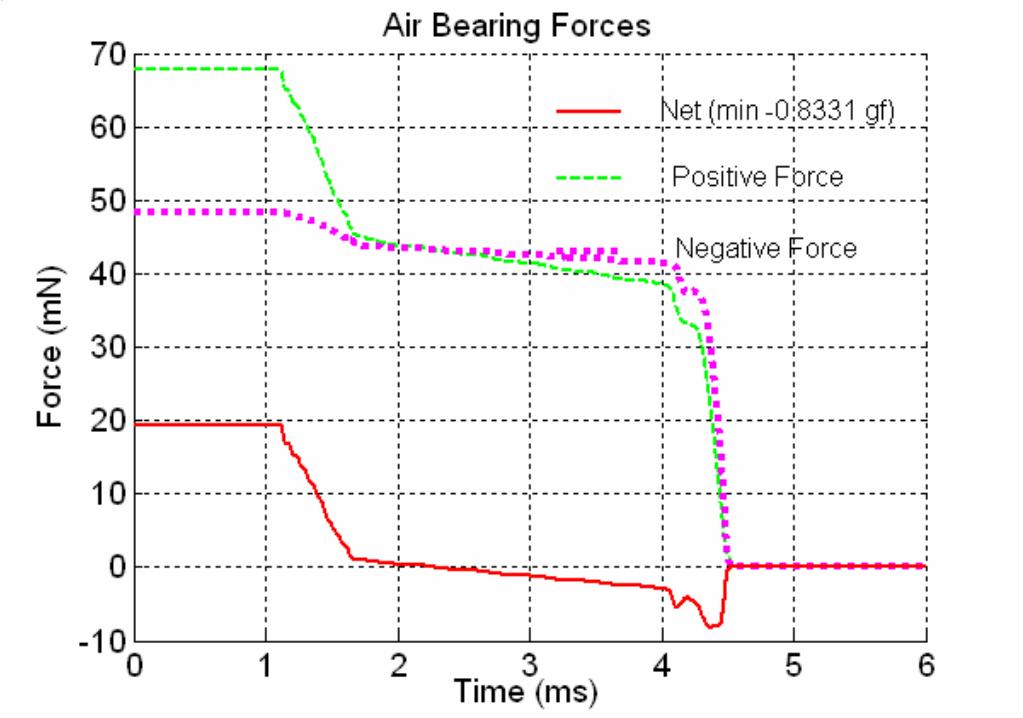

(a)

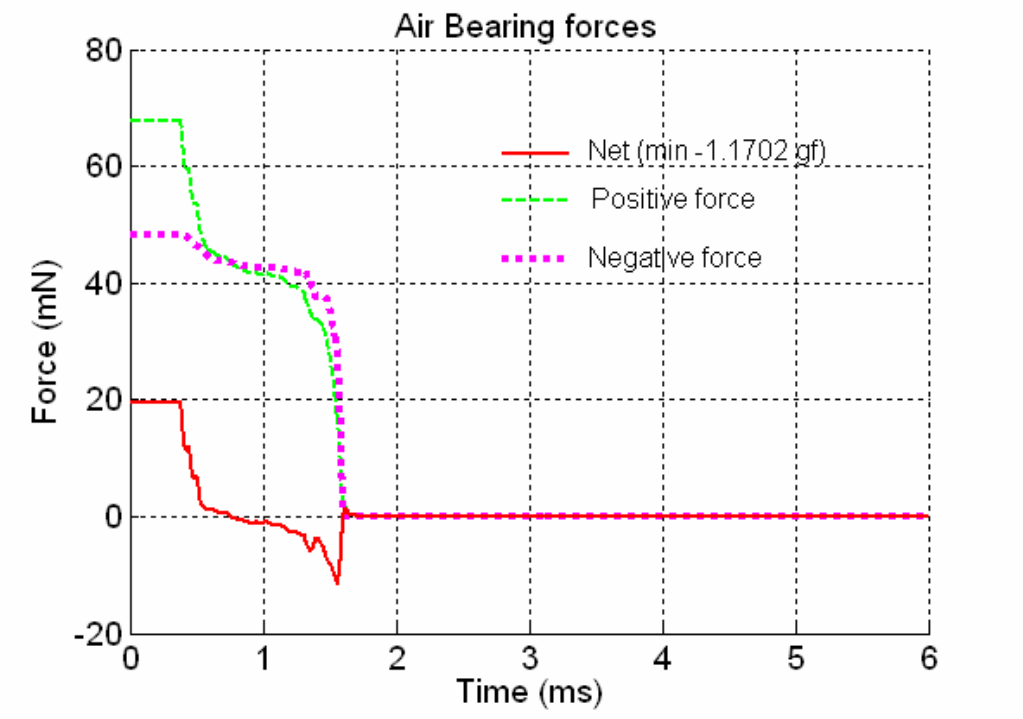

(b)

Fig. 18. Air bearing force histories during unloading processes at the OD. (a) unloading velocity: 50 mm/s; (b) 150 mm/s.

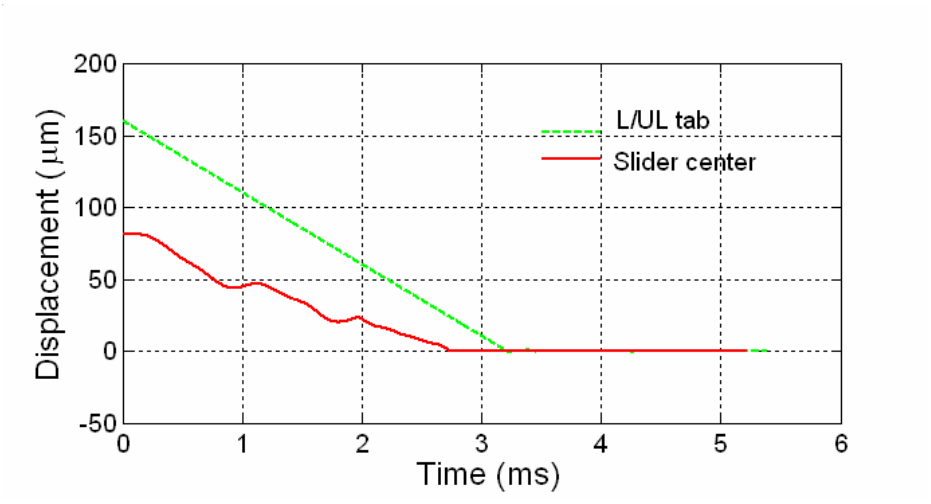

(a)

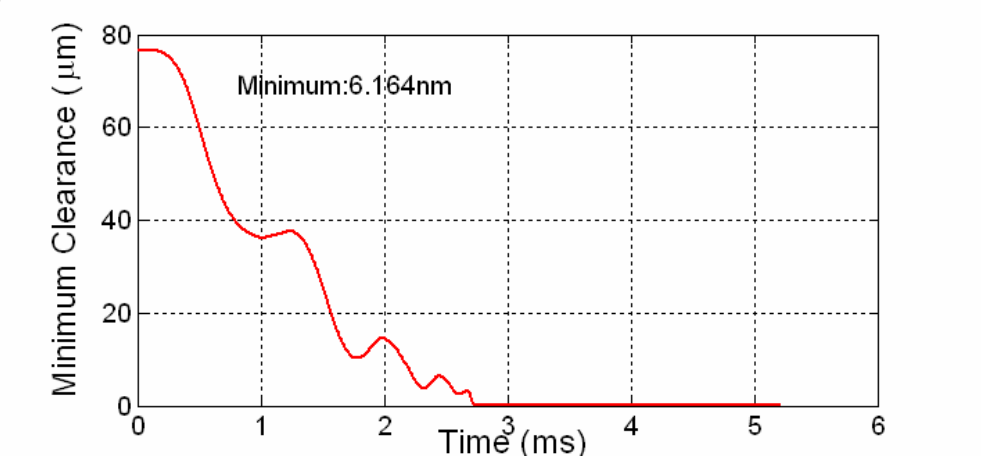

(b)

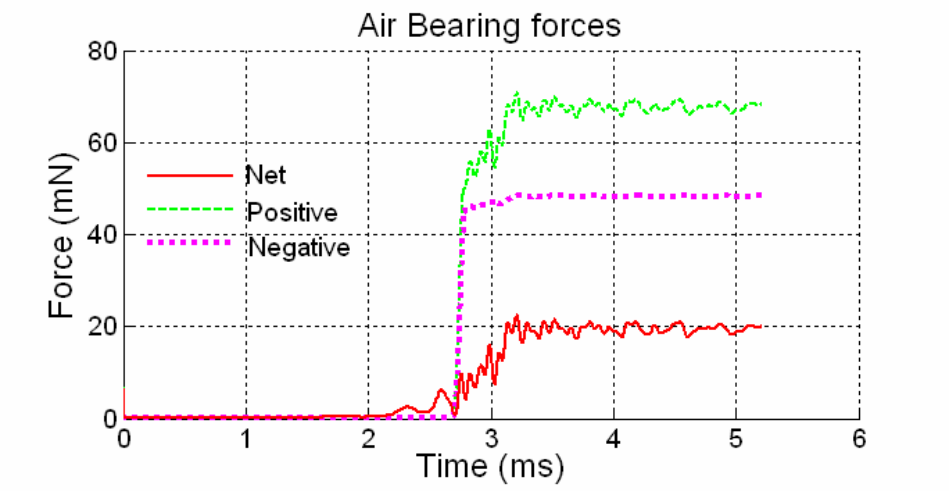

(c)

Fig. 19. Displacement, minimum clearance and force histories during loading at the OD with 50 mm/s loading velocity and 15000 rpm disk velocity.

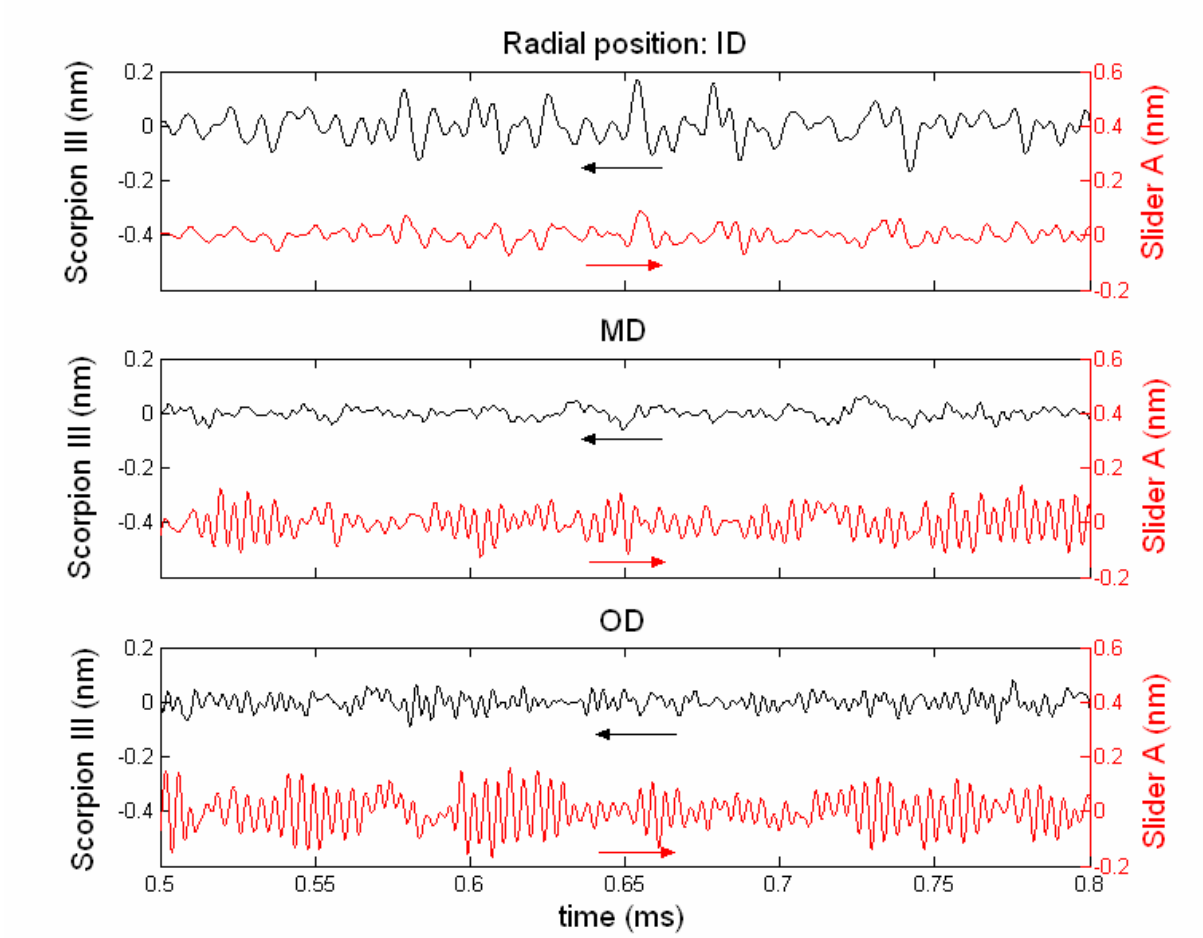

Fig. 20. Comparison of FHMs of Scorpion III and Slider A at three radial positions, ID, MD, and OD with skews -15.62˚, -2.56˚, and 7.22˚, respectively.